NANO LETTERS

Cite This: Nano Lett. 2018, 18, 2751 2758

Letter

pubs.acs.org/NanoLett

Ferroelectric Control of the Spin Texture in GeTe

Christian Rinaldi,*[,†,‡] Sara Varotto,[†] Marco Asa,[†] Jagoda Sławińska,[§] Jun Fujii,[∥] Giovanni Vinai,[∥] Stefano Cecchi,[⊥] Domenico Di Sante,[#] Raffaella Calarco,[⊥] Ivana Vobornik,[∥] Giancarlo Panaccione,[∥] Silvia Picozzi,[§] and Riccardo Bertacco*[,†,‡]

[†]Department of Physics, Politecnico di Milano, 20133 Milano, Italy

[‡]IFN CNR, Politecnico di Milano, 20133 Milano, Italy

[§]Consiglio Nazionale delle Ricerche CNR SPIN, Sede Temporanea di Chieti, c/o Univ. "G. D'Annunzio", 66100 Chieti, Italy

[∥]CNR IOM, Laboratorio TASC in Area Science Park Basovizza, 34149 Trieste, Italy

[⊥]Paul Drude Institut für Festkörperelektronik, Hausvogteiplatz 5 7, 10117 Berlin, Germany

[#]Institut für Theoretische Physik und Astrophysik, Universität Würzburg, Am Hubland Campus Süd, Würzburg 97074, Germany

Supporting Information

ABSTRACT: The electric and nonvolatile control of the spin texture in semiconductors would represent a fundamental step toward novel electronic devices combining memory and computing functionalities. Recently, GeTe has been theoretically proposed as the father compound of a new class of materials, namely ferroelectric Rashba semiconductors. They display bulk bands with giant Rashba like splitting due to the inversion symmetry breaking arising from the ferroelectric polarization, thus allowing for the ferroelectric control of the spin. Here, we provide the experimental demonstration of the correlation between ferroelectricity and spin texture. A surface engineering strategy is used to set two opposite predefined uniform ferroelectric polarizations, inward and outward, as monitored by piezoresponse force microscopy. Spin and angular resolved photoemission experiments show that these GeTe(111) surfaces display opposite sense of circulation of spin in bulk Rashba bands. Furthermore, we demonstrate the crafting of nonvolatile ferroelectric patterns in GeTe films at the nanoscale by using the conductive tip of an atomic force microscope. Based on the intimate link between ferroelectric polarization and spin in GeTe, ferroelectric patterning paves the way to the investigation of devices with engineered spin configurations.

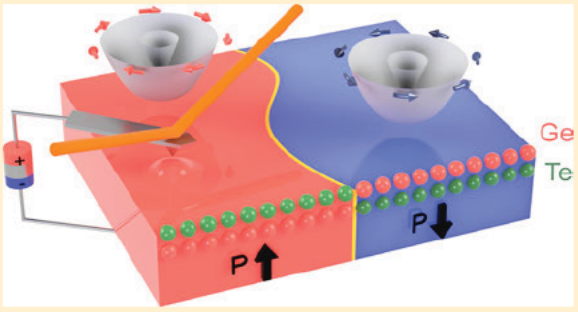

KEYWORDS: *Germanium telluride, Rashba effect, ferroelectricity, spin−orbitronics*

While Moore's law seems to approach its limit of validity, the search for new paradigms allowing the further improvement of the computing capabilities of electronic devices is entering a final rush. Spintronics is a promising route in this perspective, but so far, its success stories are limited to the field of memories. To enter the area of computing, devices capable of manipulating the information encoded in the spin are needed. In this sense, a lot of effort is currently carried out in the fields of spin logic,[1] magnon spintronics,[2,3] and semiconductor spintronics.[4−7] Nevertheless, about 20 years after the pioneering idea of "spin transistor" proposed by Datta and Das,[8] many practical limitations still prevent the implementation of effective transistors based on spin properties.[9] The dream remains to manipulate spins within semiconductors devices to exploit the full potential of materials with a gap for charge control, without use of auxiliary ferromagnetic materials and magnetic fields. Beyond magnetic semiconductors,[10] which still suffer from low temperature operation and the need of external magnetic fields to control the spin texture, new materials and concepts are necessary. In this context, the recently introduced class of ferroelectric Rashba semiconductors (FERSCs),[11] whose father compound is α GeTe,[12] is highly promising. They are semiconductors and also ferroelectrics, so that the remanent ferroelectric polarization vector breaks the inversion symmetry and determines a giant bulk Rashba k dependent spin splitting of the bands.[13] Remarkably, density functional theory (DFT) simulations predict that the spin direction in each sub band should reverse upon inversion of the ferroelectric polarization, thereby allowing its electrical control. In perspective, these unique features could be exploited in novel devices[14,15] integrating memory and computing functionalities within the very same channel of a spin transistor.[16] While ferroelectric hysteresis provides the memory functionality, spin dependent transport phenomena in spin textures defined by ferroelectric domains can implement computing, within the very same devices.

Received: November 15, 2017
Revised: January 20, 2018
Published: January 30, 2018

DOI: 10.1021/acs.nanolett.7b04829
Nano Lett. 2018, 18, 2751−2758

In this paper, we address a fundamental issue on the roadmap toward the exploitation of FERSCs: the nonvolatile, but reversible, electric control of the spin texture in α GeTe thin films down to the nanoscale, thus paving the way to the definition of unconventional spin configurations in semi conductors. The electric switching of the ferroelectric (FE) polarization has been already demonstrated in GeTe(111) films[13] and more recently in GeTe nanowires.[17] However, an experimental proof of the reversal of the spin texture (the clockwise or counterclockwise sense of circulation of spins in bulk Rashba like bands) for opposite FE polarization is still missing. So far, only a link between the direction of the FE polarization and the spin orientation in the surface Rashba sub bands has been reported.[13] More recently, the impact of magnetic fields on the spin texture of Mn doped GeTe films has been investigated but always for fixed FE polarization.[18]

Here, we experimentally establish the intimate link between the orientation of the remanent ferroelectric polarization and the circulation of spin texture associated with Rashba bands in GeTe(111) thin films. First, we describe a surface engineering strategy to prepare in situ α GeTe(111) films with uniform pristine ferroelectric polarization, outward or inward. Then, by spin and angular resolved photoemission spectroscopy (S ARPES), we provide evidence for opposite sense of spin circulation of bulk Rashba bands in the two surfaces prepared with opposite FE polarization. Our results suggest the possibility of crafting the spin texture at the nanoscale in GeTe via ferroelectric patterning. In this route, we demonstrate the reversible writing of an array of nanostripes with inward and outward FE polarization, assumed to have opposite spin configurations. This represents a first example of engineered meta material based on a ferroelectric Rashba semiconductor, suitable to implement the concept of Rashba barriers. In perspective, our results pave the way to the exploitation of GeTe in unconventional spintronic devices with pure electric control of their operation and reconfigurable computing functionalities.

The first step toward the demonstration of the link between FE state and spin texture in GeTe by S ARPES is the initialization of the whole film, leading to a uniform pristine FE polarization pointing inward or outward. This also corresponds to the "clean blackboard" state preliminary to any patterning. In this scope, we developed a method for preparing α GeTe(111) surfaces with opposite FE polarization, associated with different terminations. Rhombohedral α GeTe(111) results from the stacking of Ge and Te planes, which are not equidistant and thus give rise to a net electric dipole, being Te more electronegative than Ge.[19,20]

As the energetically favored termination is generated by the breaking of long (rather than short) bonds, a Te terminated surface is expected to display a dipole pointing outward (P_{out}), while a Ge terminated one will have a net dipole inward (P_{in}), as depicted in panels a and a′ of Figure 1. Even though calculations predict the Te terminated GeTe(111) to be more stable than the Ge terminated one by 60 meV Å^{-2}, this surface energy difference is largely reduced by the presence of reconstructions,[21] vacancies, and other kind of defects, thus suggesting the possibility of stabilizing both terminations in real surfaces.

GeTe(111) films, 23 nm thick, were grown by molecular beam epitaxy (MBE) on Si(111) and then capped with 20 nm of Te to prevent contamination due to exposure to atmosphere. A reliable protocol for controlled Te desorption in ultrahigh

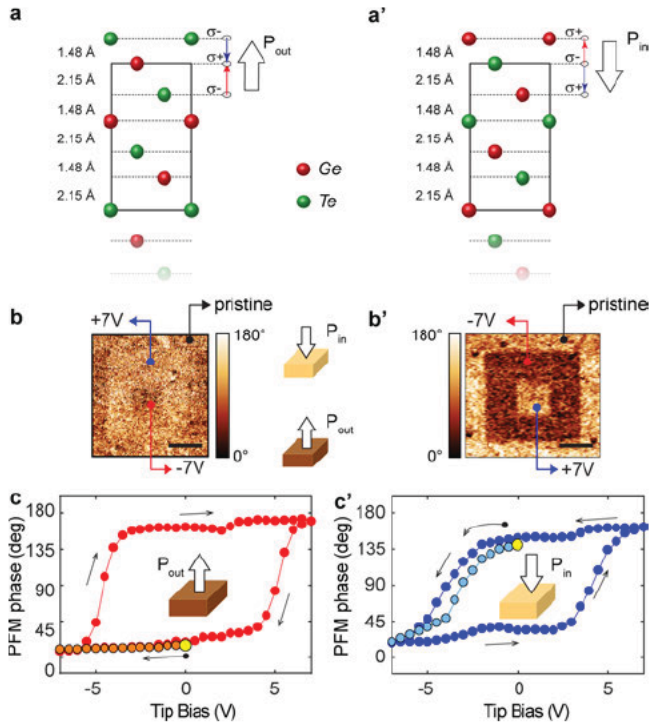

Figure 1. GeTe(111) surfaces with opposite FE polarization. (a, a′) Sketch of the Ge and Te planes for the Te and Ge termination, respectively. The distances given on the left refer to the unrelaxed interlayer distances. Only the topmost surface atoms of the slab are shown. The black rectangle denotes a bulk hexagonal unit cell used in DFT calculations as a building block to construct the (111) surface (rhombohedral setting, corresponding to the (0001) in the hexagonal setting). The net FE polarization P_{out} (P_{in}) (white arrows) arises from the interatomic dipoles shown with blue and red arrows. (b, b′) Piezoresponse phase images recorded on S_{Te} (S_{Ge}) after poling with the tip at +7 V (−7 V) and −7 V (+7 V) over two concentric squares of 1.5 and 0.5 μm per side. The scale bar corresponds to 0.5 μm. (c, c′) PFM phase signal showing the pristine polarization state and the ferroelectric hysteresis loop, as measured ex situ on S_{Te} and S_{Ge} after the S ARPES experiment. The controlled thermal desorption of the Te capping layer leads to a virgin state FE polarization P_{out} and P_{in} in the two samples, respectively.

vacuum (UHV) has been first optimized to obtain Ge and Te rich surfaces with opposite polarization, as checked by X ray photoemission spectroscopy (XPS) with Al−Kα radiation and piezoresponse force microscopy (PFM) (for details, see sections 1 and 2 of the Supporting Information). An annealing of 1 h at about 240 °C produces a Te rich surface displaying a pristine polarization P_{out}, while the same annealing at 260 °C causes a complete desorption of Te (the more volatile species) and produces a Ge rich surface with P_{in}. Crucial for this paper, the same method has been applied to samples prepared in situ for S ARPES, to demonstrate that opposite FE polarization states are associated with inverse spin texture. After insertion in vacuum at the APE beamline, the samples were annealed at about 240 and 260 °C for 1 h, controlling the heater current. According to the recipe previously optimized (for details see section 2 of the Supporting Information), we obtained a first sample (S_{Te}) with a Te rich surface and a second one (S_{Ge}) with a Ge rich surface, as confirmed by the in situ analysis of the XPS spectra taken at 800 eV photon energy (see section 3 of the Supporting Information). In fact, from the relative intensity of the Ge 3d and Te 4d peaks, normalized to the

DOI: 10.1021/acs.nanolett.7b04829
Nano Lett. 2018, 18, 2751−2758

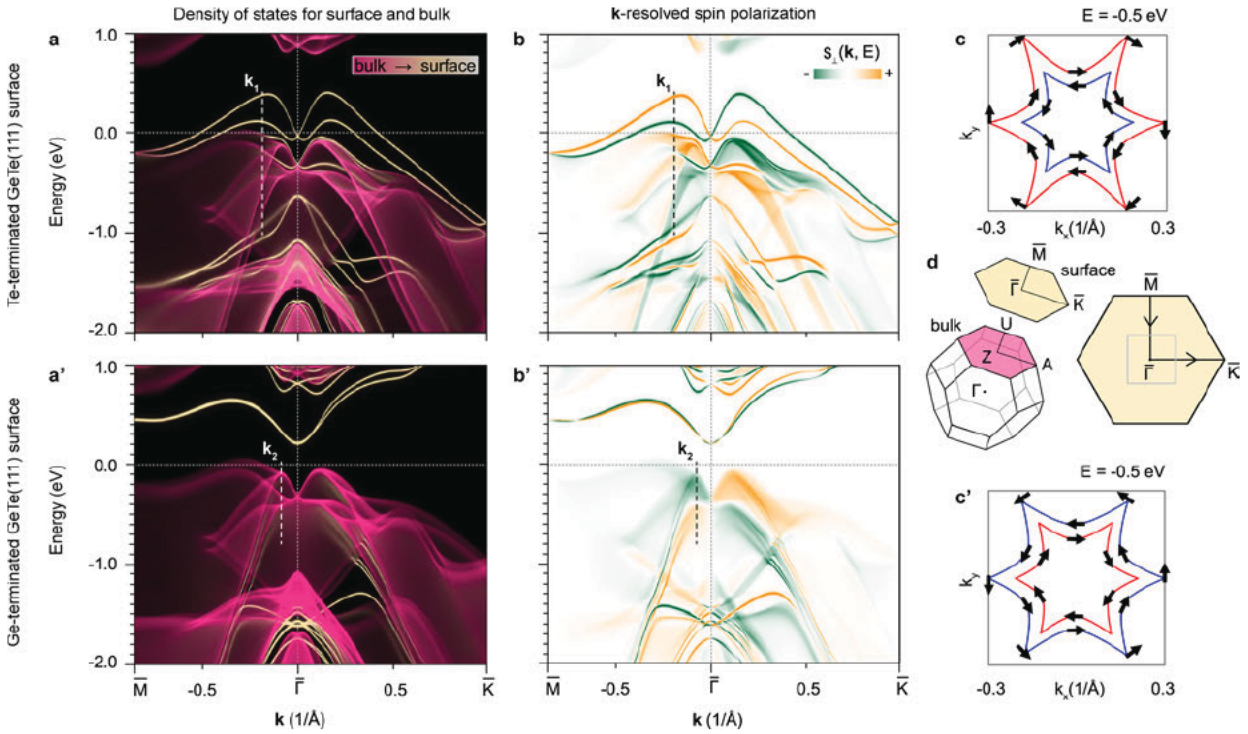

Figure 2. DFT calculations of GeTe(111) surfaces with different terminations. (a) Density of states (spectral function) of Te terminated GeTe(111) surface with outward polarization, projected on bulk (deep pink) and surface (yellow) principal layers calculated via Green's functions technique for the semi infinite model of the surface. Brighter tones of pink (yellow) bands indicate higher intensity of bulk (surface) features. High symmetry directions used for the calculation of band dispersions are defined in panel d. (b) Corresponding **k** resolved spin polarization along the high symmetry directions. Due to its complexity, we show only the in plane components perpendicular to **k**. The in plane component parallel to wave vector is zero within the whole Brillouin zone. (c) Schematic picture of the spin texture in main bulk bands extracted from panels a and b at $E = -0.5$ eV; the arrows denote the direction of the in plane projection of the spin for inner and outer bands. (a′−c′) Same as panels a−c for Ge terminated surface, with polarization inward. The Fermi level here has been shifted to align the bulk bands of Te and Ge terminated surfaces. (d) Brillouin zone of hexagonal surface and bulk unit cells; the gray square marks the area displayed in panels c and c′. Dashed vertical lines in a and a′ indicate the k points used for the spin analysis reported in Figure 4.

analyzer transmission and tabulated atomic photoemission cross sections, the average stoichiometries of S_{Te} and S_{Ge} are $Ge_{0.39}Te_{0.61}$ and $Ge_{0.46}Te_{0.54}$, respectively. The uncertainty on the relative stoichiometry is ± 0.02, and it mainly arises from the error on the estimation of the peaks' area. Within the photoemission probing depth (~17 Å at 800 eV photon energy), S_{Te} is clearly Te rich, while the Ge concentration in S_{Ge} is slightly above that of GeTe films, which typically displays 10% Ge vacancies ($Ge_{0.45}Te_{0.55}$),[22,23] thus pointing toward a Ge enrichment of S_{Ge}. Data taken with Al−Kα radiation (1486.6 eV), after the beamtime, confirm that S_{Te} (S_{Ge}) is Te (Ge) rich at surface (see section 2 of the Supporting Information). Furthermore, the deconvolution of XPS spectra, using surface and bulk components (section 2 of the Supporting Information), shows that the Te (Ge) enrichment is localized at surface. Based on these considerations, in the following we will compare our ARPES data from S_{Te} and S_{Ge} with density functional theory simulations of Ge and Te terminated surfaces. In fact, these truncated bulk systems represent the simplest models of Te and Ge rich surfaces with outward and inward FE polarization.

The virgin ferroelectric state of Te and Ge rich samples has been widely investigated by PFM, both during the optimization of the surface strategy for poling (section 1 of the Supporting Information) and after the beamtime, on samples S_{Te} and S_{Ge}. Here in particular, we report on these two samples, whose pristine FE state is crucial for the establishment of the link between FE polarization and spin texture. In Figure 1b (1b′), we show the phase signal recorded on S_{Te} (S_{Ge}) after writing a large square with +7 V (−7 V) bias on the AFM tip and then an inner square with opposite bias. FE patterns are stable over more than 24 h (section 1 of the Supporting Information), thus indicating the robustness of ferroelectricity in GeTe films. The inner square displays the same contrast (PFM phase) of the unpoled area, indicating an outward (inward) virgin ferro electric polarization in S_{Te} (S_{Ge}). To confirm these findings, we measured the virgin curve and the full ferroelectric hysteresis loops by sweeping the PFM tip voltage. A pair of characteristic loops measured on S_{Te} and S_{Ge} are reported in panels c and c′ of Figure 1 as representative of the average response of the entire sample area probed by S ARPES (see section 1 of the Supporting Information for details on the statistical analysis). The virgin curve measured for S_{Te} indicates the initial state is close to that obtained for negative saturating voltages, while the opposite holds for the sample S_{Ge}. This is a clear indication that S_{Te} and S_{Ge} present two opposite outward and inward virgin FE polarizations. These samples are ideal candidates for investigat ing the connection between FE polarization and spin texture.

In Figure 2, we show the bands dispersion and the corresponding spin texture calculated by DFT for Te and Ge terminated GeTe(111) surfaces displaying, respectively, P_{out} and P_{in} FE polarization that will be compared with S ARPES from S_{Te} (Te rich surface) and S_{Ge} (Ge rich surface), respectively. For the sake of completeness, the spectral function

DOI: 10.1021/acs.nanolett.7b04829
Nano Lett. 2018, 18, 2751−2758

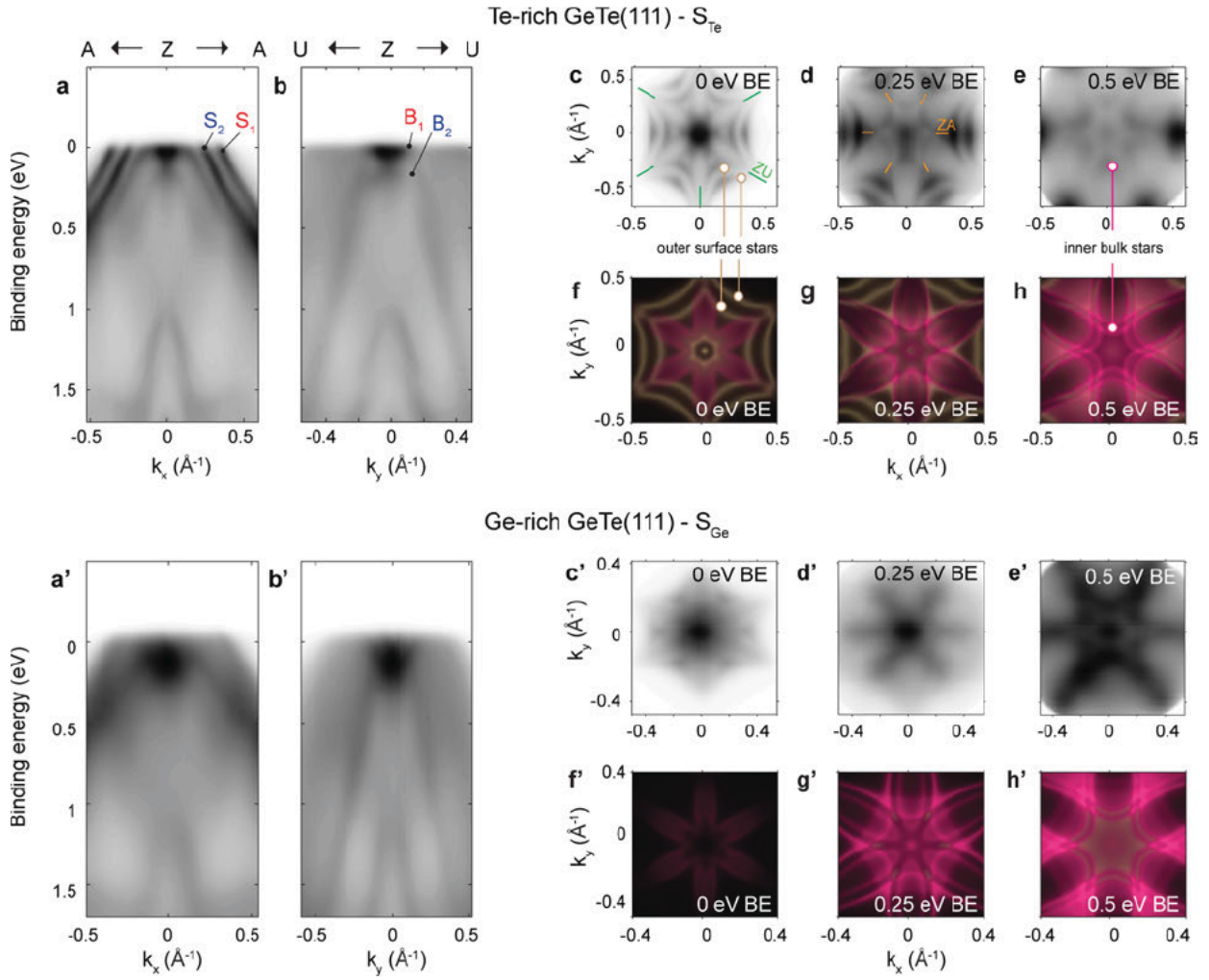

Figure 3. ARPES from Te rich and Ge rich samples. Panels a−h refer to the Te rich sample S_{Te} with outward polarization. (a, b) Experimental bands dispersion collected along the principal directions ZA (k_x) and ZU (k_y) in the Brillouin zone. (c−e) Constant energy maps at 0, 0.25, and 0.5 eV below the Fermi energy. (f−h) Corresponding calculated constant energy maps with yellow and pink indicating the surface and bulk character of states, respectively. Panels labeled by the apex (panels a′−h′) are the same as above but for the Ge rich sample S_{Ge} with inward polarization. The Fermi level in panels f′−h′ is chosen to be consistent with Figure 2.

for the energetically unfavorable configurations (i.e., Te terminated surface with P_{in} and Ge terminated surface with P_{out}) are reported in section 3 of the Supporting Information. In agreement with previous works,[21,24] we refer to bulk coordinates in terms of the rhombohedral setting ($a = b = c = 4.37$ Å and $\alpha = \beta = \gamma = 57.9°$), such that the ferroelectric polarization points along the [111] direction of the real space and the Rashba like dispersion of bulk bands is seen on the {111} planes of the reciprocal space around Z. However, to simulate surface aspects we adopt the more common hexagonal setting to construct the slabs (Figure 1, panels a and a′), with the ferroelectric polarization pointing along the [0001] direction. However, throughout the text, we will refer to the sample surface as GeTe(111) defined with respect to the rhombohedral cell.

The bulk high symmetry directions ZU and ZA, together with the corresponding surface directions $\overline{\Gamma M}$ and $\overline{\Gamma K}$, are shown in Figure 2d. The FE polarization is parallel to ΓZ direction of the reciprocal space, i.e., the (111) direction of the crystal. Band dispersions along high symmetry directions are presented in Figure 2a for S_{Te} and Figure 2a′ for S_{Ge}, after projection of the spectral function on the surface layers and on the bulk in the semi infinite model, to single out surface and bulk like contributions.

The k resolved spin polarization is reported in panel b for S_{Te} and b′ for S_{Ge}, in which the non null spin components perpendicular to the wave vector are shown along the high symmetry bulk (surface) ZA ($\overline{\Gamma K}$) and ZU ($\overline{\Gamma M}$) directions. While the shape of bulk Rashba sub bands is not affected by FE polarization reversal, their spin texture is reversed, according to the main concept of FERSCs. This is evident from the comparison of the isoenergy cuts, taken at 0.5 eV below the top of the valence band, reported in panels c and c′, where arrows indicate the local spin direction. However, surface bands with Rashba splitting are very different for the two terminations. In the Te terminated one (P_{out}) they display a clear Rashba like splitting and cross the Fermi energy at higher wave vectors with respect to the bulk bands. In the Ge terminated one (P_{in}), instead, the Rashba splitting of the surface bands in the gap is largely suppressed and surface bands shift toward the conduction band, without crossing the Fermi level at high momenta.

The remarkable difference between surface Rashba like bands predicted by DFT for Te and Ge termination has an

DOI: 10.1021/acs.nanolett.7b04829
Nano Lett. 2018, 18, 2751−2758

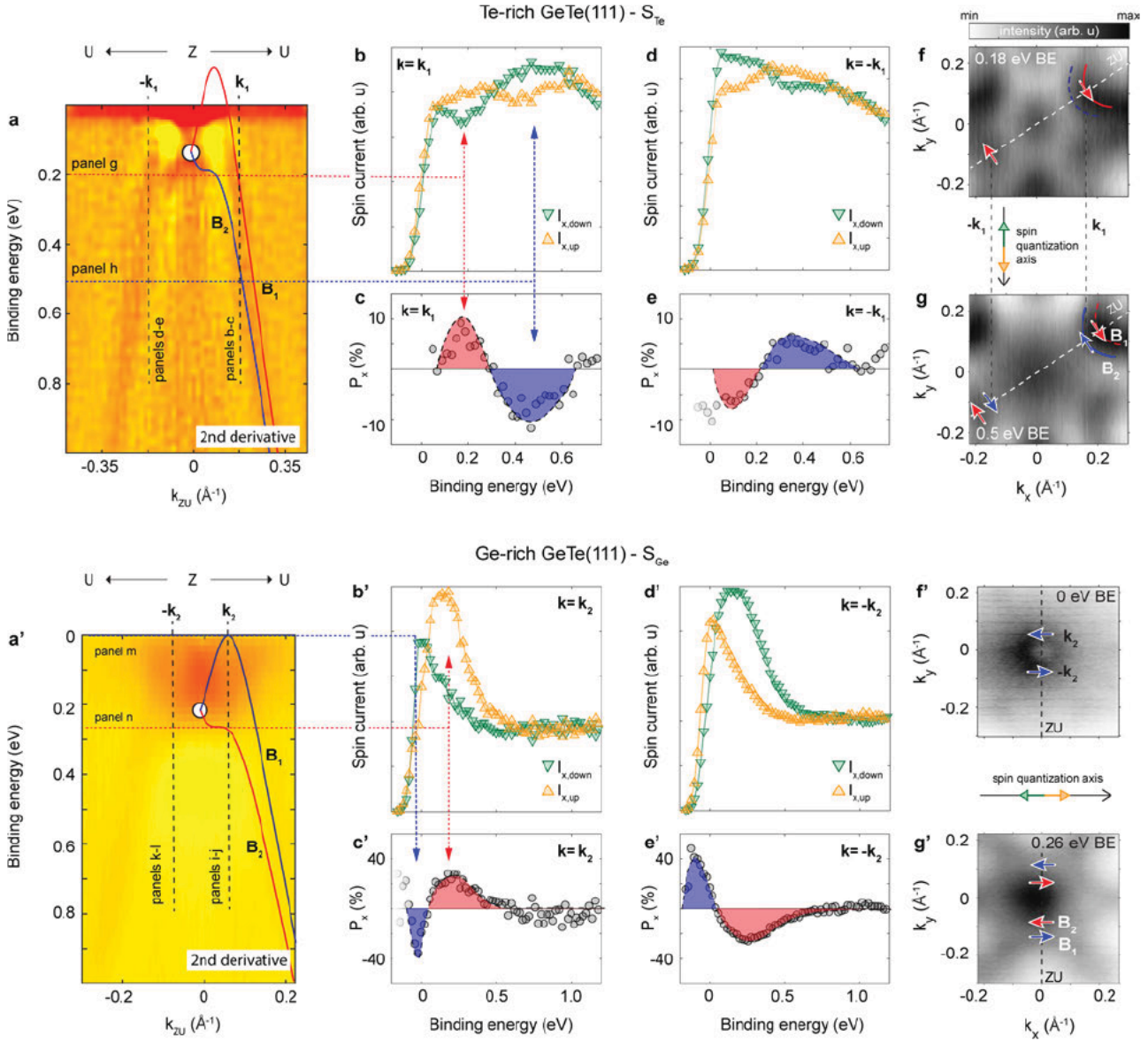

Figure 4. Spin resolved ARPES from Te rich and Ge rich samples. Panels a–g refer to the Te rich sample S_{Te} with outward polarization. (a) Calculated bulk bands (solid line) along ZU (k_y) over the 2nd derivative of the measured band dispersion. (b, c) Spin polarized spectra and spin asymmetry at fixed wave vector $\mathbf{k_1}$ indicated in panel a. The two peaks correspond to the intersection of bulk Rashba bands B_1 and B_2 with the vertical dashed line at $\mathbf{k_1}$ (panel a). (d, e) Spin polarized spectra and spin asymmetry at opposite wave vector $-\mathbf{k_1}$. (f, g) Constant energy maps at 0.18 and 0.5 eV BE, corresponding to the energy of bulk bands B_1 and B_2 at $\mathbf{k_1}$, in nice agreement with the peaks of opposite spin polarizations in panels c and e. Blue and red arrows indicate the sense of circulation of spins: clockwise in the outer band and counterclockwise in the inner one. Panels a′–g′ refer to the case of the Ge rich sample S_{Ge}. (b′–e′) Spin analysis for opposite wave vectors $\mathbf{k_2}$ and $-\mathbf{k_2}$, where the Rashba splitting is maximized. (f′, g′) Constant energy maps at 0 eV (top of B1) and 0.26 eV BE, corresponding to the energy of bulk bands B_1 and B_2 at $\mathbf{k_2}$ (panel a′). The sense of circulation of spins is opposite to that found for S_{Te}: counterclockwise in the outer band and clockwise in the inner band (panel g′).

experimental counterpart in ARPES data reported in Figure 3 for S_{Te} (panels a–h) and S_{Ge} (a′–h′). Panels a and b in Figure 3 present the experimental band dispersions along ZA and ZU for S_{Te}. Corresponding isoenergy cuts at 0, 0.25, and 0.5 eV BE in panels c–e of Figure 3 are compared with theoretical ones for a Te terminated surface. In the following we will use a simplified distinction between "surface" and "bulk" Rashba states. Having in mind that ARPES at 20 eV probes just a few atomic layers underneath the sample surface, we identify as bulk states those displaying a sizable photon energy or k_z dispersion.[13] Rigorously, these are not true bulk states but can be viewed as surface bulk resonances[24] or simply states with sizable projection on bulk states, so they mainly reflect the bulk behavior.[25]

Both band dispersions and isoenergy cuts from sample S_{Te} are very similar to data available in the literature for Te terminated α GeTe(111).[13,24,25] In agreement with DFT calculations, prominent surface bands with Rashba splitting (S_1, S_2) are seen at large momenta, especially along the ZA direction. A pair of outer spin split bands with 6 fold symmetry and "arms" along the equivalent ZU directions are clearly visible in the isoenergy cuts of panels c and d of Figure 3 (marked by green ticks). However, at 0.25 eV BE (Figure 3d), an inner 6 fold star (orange ticks) appears, rotated by 30 degrees with respect to the surface one, i.e., with arms along

DOI: 10.1021/acs.nanolett.7b04829
Nano Lett. 2018, 18, 2751–2758

ZA. This is ascribed to the bulk like bands (B_1 and B_2) evident in the band dispersion along ZU of panel b. The isoenergy cut at 0.5 eV (Figure 3e), instead, mainly reflects the symmetry of the bulk inner star because at this BE, the cut of states with surface character occurs at higher momenta.

The scenario for the S_{Ge} sample is completely different because surface states are almost absent, in agreement with DFT simulations. Indeed the prominent surface Rashba bands S_1 and S_2 along ZA in Figure 3a are missing in panel a′, while bulk bands B_1 and B_2 along ZU[12] are similar in panels b and b′. The absence of S_1 and S_2 surface states is even more evident from the Fermi energy cut of panel 3c′, which does not display the outer 6 fold double star of panel c. Besides, the isoenergy cut at 0.25 eV (panel d′) already reflects the symmetry of bulk states, such as the inner star in Figure 3d,e from sample S_{Te}, i.e., with arms along ZA.

To summarize, ARPES data from samples S_{Te} and S_{Ge} show band dispersions in good agreement with those calculated for a Te terminated (P_{out}) and Ge terminated (P_{in}) surface, respectively. This represents a self consistent proof of the reliability of our method for preparing GeTe(111) surfaces with opposite FE polarization.

In the following, we discuss the connection between the spin texture of bulk Rashba bands and the FE polarization, which is the key concept of FERSC materials. Figure 4 reports spin resolved ARPES data from S_{Te} and S_{Ge}.

In fact, the Rashba splitting of surface bands can be largely affected, or even suppressed, by proximity with other materials in a multilayer[26] or by the surface electric field due to screening charges. In sample S_{Te}, which displays both surface and bulk Rashba bands, we performed spin polarized scans at fixed momenta (k_1, $-k_1$) marked in panels f and g of Figure 4, along the equivalent ZU direction at 30 degrees with respect to k_x. Even though these are not the points where the Rashba splitting is maximized, for $\pm k_1$, only bulk bands $B_{1,2}$ are expected to contribute to the photoemission signal at BE greater than 0.2 eV (see Figure 2a,b). The spin polarized spectra and corresponding spin polarization are reported in panels b and c for k_1 and d and e for $-k_1$. With reference to the polarimeter quantization axis set along the negative direction of k_y, at k_1, we find a positive peak in the spin polarization at about 0.2 eV and a negative one at about 0.5 eV (panel c), corresponding to the crossing of the outer and inner band B_1 and B_2, respectively. The opposite occurs at $-k_1$, as expected for GeTe Rashba bands.[12,24,25] The sense of circulation of spins resulting from our data is sketched in Figure 4f,g by arrows superimposed to the isoenergy cuts taken at 0.18 and 0.5 eV. In agreement with DFT calculations, for a Te terminated (P_{out}) surface the sense of circulation of spins is clockwise for the outer band and counterclockwise for the inner one.

For S_{Ge}, the analysis of the spin texture of bulk bands is simpler, due to the lack of surface bands. In this case, we choose opposite k points (k_2, $-k_2$), along k_y (ZU direction), where the maximum Rashba energy splitting (E_R) of bulk bands $B_{1,2}$ is expected (see Figures 2a′ and 4a′). The quantization axis of the spin polarimeter was set orthogonal to the wave vectors toward the positive k_x direction. Spin polarized spectra in Figure 4b′ display two prominent peaks with opposite spin, arising from the crossing of B_1 and B_2 bands at k_2. Their energy splitting of about 200 meV is in good agreement with the expected value of the Rashba energy E_R, according to theoretical predictions[12] and recent experimental findings.[24,25] Noteworthy is the fact that the sign of the spin polarization of the two peaks reverts when moving from k_2 to $-k_2$, as it appears from the comparison of panels b′−e′ in Figure 4. To determine the sense of circulation of spins in the outer and inner bands, we simply note that in panel c′, the peak at lower BE (outer band) has a negative polarization with respect to the quantization axis, i.e., the spin is directed along the negative direction of k_x (counterclockwise rotation). The opposite holds for the peak at higher BE (inner band), so that the sense of circulation of the spin there is clockwise. The corresponding spin texture is sketched in panels f′ and g′. For a more detailed vectorial analysis of the spin texture, see section 4 of the Supporting Information.

Crucial for the demonstration of the basic concept of FERSCs, the sense of circulation of spin in the inner and outer bands is opposite in samples S_{Te} (Figure 4g) and S_{Ge} (Figure 4g′), which display outward and inward FE polarization, respectively. This means that the spin texture is locked to the FE polarization because it reverts when the FE polarization is switched.

Having demonstrated the locking between ferroelectric polarization and spin textures, in the following we focus on the nanopatterning of ferroelectric domains. Figure 5 reports an example of a peculiar ferroelectric pattern written in a GeTe film, i.e., an array of lines with 600 nm spacing, having FE polarization inward (P_{in}), in a sample with uniform FE polarization outward (P_{out}). This pattern has been defined starting from a sample with uniform P_{out}, obtained by applying the surface engineering method outlined above for producing a Te rich surface, over which a sequence of lines with opposite polarization has been written by sweeping the conductive tip of the AFM with a positive bias of +10 V. For a sweep rate of 3 μm/s, we get an average line width of about 300 nm as a result of the characteristic GeTe FE viscosity.

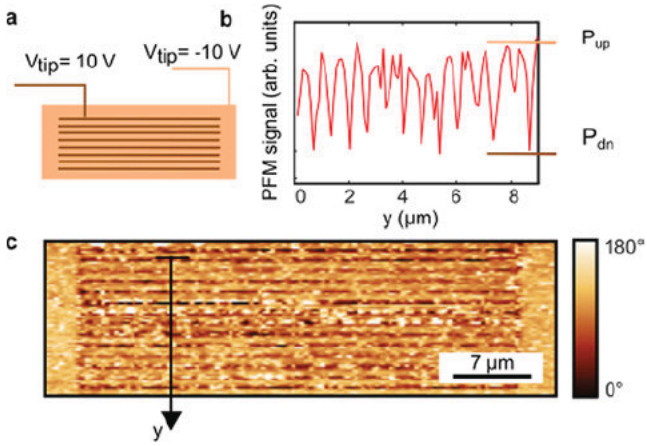

Figure 5. FE domains and spin texture patterning at the nanoscale. (a) Sketch of the writing procedure to obtain a sequence of Rashba barriers using the conductive tip of an AFM on a sample with pristine polarization outward, prepared as for sample S_{Te} above or by sweeping the tip with a negative voltage (V_{tip} = −10 V). Lines of inward polarization are written with opposite bias (V_{tip} = 10 V). The distance between lines is 600 nm, and their width about 300 nm. (b) PFM phase signal measured along the y direction, perpendicular to the lines. (c) PFM phase image of the ferroelectric domain pattern.

It is noteworthy that the pattern is stable over more than 24 h, thus pointing to the possibility of using this kind of FE patterns in spintronic devices exploiting the propagation of electrons in structure with engineered in plane domains with

DOI: 10.1021/acs.nanolett.7b04829
Nano Lett. 2018, 18, 2751−2758

opposite spin texture. Even though the direct observation of the spin in these FE nanodomains is prevented by experimental limitations of spectroscopic techniques, our S ARPES analysis indicates that patterning of FE domains with inward or outward polarization provides a way to define also spin textures with opposite sense of rotation of spins in the Rashba bands. The FE structure of Figure 5 thus corresponds to the typical Rashba barrier device, where lines with opposite FE polarization are associated with opposite sense of circulation of spins in the Rashba bands. According to the theory of Rashba barriers,[27−29] a modulation of the resistivity for current flowing perpendic ularly to the lines is expected with respect to the case of uniform FE polarization. Noteworthy, such a modulation is nonvolatile but reversible, as the uniform polarization state can be restored by electric poling. In perspective, similar structures can be designed and implemented in devices with gate electrodes, suitable for an easy and real time manipulation of the spin texture and, in turn, of the electric conductivity. This represents the basic building block of a circuit element combining memory and computing, where the information is written in the nonvolatile ferroelectric and spin texture pattern and computing takes place via the modulation of some spin dependent transport property.

To summarize, in this Letter, we demonstrated the ferroelectric control of the spin texture in GeTe. We developed a surface engineering strategy to prepare in situ a uniform ferroelectric polarization state, inward or outward. Through S ARPES, we provided evidence for the intimate correlation between ferroelectric polarization and spin circulation in Rashba bands, i.e., the basis toward the possibility of crafting the spin texture via ferroelectric patterning. In this direction, by using the conductive tip of an atomic force microscope, we wrote a sequence of ferroelectric domains with inward and outward polarization expected to implement the structure of a Rashba barrier device. Noteworthy, FE domains are stable over time but can be electrically manipulated in a reversible way. These achievements pave the way to the realization of devices with gate electrodes for the real time reconfiguration of the spin structure in view of computing applications. Our findings indicate that a full electric control of the spin in a semiconductor is feasible without magnetic fields or adjacent magnetic layers. This represents a fundamental achievement toward the deployment of GeTe in spintronic devices exploiting the rich physics of Rashba effect and the additional degree of freedom arising from the electric reconfigurability of the spin texture.

■ ASSOCIATED CONTENT

● Supporting Information

The Supporting Information is available free of charge on the ACS Publications website at DOI: 10.1021/acs.nanolett.7b04829.

Additional information about the methods (sample growth, DFT calculations, angular resolved photo emission spectroscopy, and piezoresponse force micros copy), engineering of Te and Ge rich GeTe(111) surfaces with opposite polarization, detailed XPS characterization of Te rich and Ge rich samples, vectorial analysis of the spin texture of GeTe, and DFT calculations of GeTe(111) surfaces with unstable terminations. (PDF)

■ AUTHOR INFORMATION

Corresponding Authors

*E mail: christian.rinaldi@polimi.it. Phone: +39 02 2399 9661.
*E mail: riccardo.bertacco@polimi.it. Phone: +39 02 2399 9663.

ORCID

Christian Rinaldi: 0000 0001 6930 211X
Giovanni Vinai: 0000 0003 4882 663X
Stefano Cecchi: 0000 0002 2243 7268
Raffaella Calarco: 0000 0002 5008 1617

Author Contributions

R.B. conceived the experiment and coordinated the research work with the help of C.R.; S.C. and R.C. planned the GeTe sample growth; S.C performed the growth and structural characterization. C.R. and S.V. optimized the surface engineer ing strategy and performed PFM experiments. C.R., S.V., M.A., and R.B. carried out S ARPES and XPS experiments. J.F., G.V., and G.P. provided assistance during the beamtime. J.S., D.D.S., and S.P. performed DFT calculations. R.B., C.R., G.P., I.V., J.S., and S.P. wrote the paper.

Notes

The authors declare no competing financial interest.

■ ACKNOWLEDGMENTS

We are grateful for helpful discussions with G. Rossi and M. Cantoni. C.R., S.V., M.A., and R.B. acknowledge financial support by the Cariplo Foundation grant no. 2013 0726 (MAGISTER) and grant no. 2013 0623 (SEARCH IV). C.R. also acknowledge the financial support by Fondazione Cariplo and Regione Lombardia via the project ECOS (grant no. 2017 1622). This work has been partly performed in the framework of the nanoscience foundry and fine analysis (NFFA MIUR Italy) project. R.C. and S.C. thank S. Behnke and C. Stemmler for technical support at the MBE and the Leibniz Gemeinschaft within the Leibniz Competition on a project entitled "Epitaxial phase change superlattices designed for investigation of non thermal switching" for partial funding. D.D.S. acknowledges the Deutsche Forschungsgemeinschaft (SFB 1170 ToCoTronics) and the ERC StG 336012 Thomale TOPOLECTRICS. This work was partially performed at Polifab, the micro and nanofabrication facility of Politecnico di Milano.

■ REFERENCES

(1) Allwood, D. A. *Science (Washington, DC, U. S.)* **2005**, *309* (5741), 1688−1692.
(2) Karenowska, A. D.; Chumak, A. V.; Serga, A. A.; Hillebrands, B. *Handbook of Spintronics*; Springer: Dordrecht Heidelberg; 2015; Vol. *11*, pp 1505−1549.
(3) Albisetti, E.; Petti, D.; Pancaldi, M.; Madami, M.; Tacchi, S.; Curtis, J.; King, W. P.; Papp, A.; Csaba, G.; Porod, W.; Vavassori, P.; Riedo, E.; Bertacco, R. *Nat. Nanotechnol.* **2016**, *11* (6), 545−551.
(4) Jansen, R. *Nat. Mater.* **2012**, *11* (5), 400−408.
(5) Rinaldi, C.; Cantoni, M.; Petti, D.; Sottocorno, A.; Leone, M.; Caffrey, N. M.; Sanvito, S.; Bertacco, R. *Adv. Mater.* **2012**, *24* (22), 3037−3041.
(6) Sanvito, S. *Nat. Phys.* **2010**, *6* (8), 562−564.
(7) Ciudad, D.; Gobbi, M.; Kinane, C. J.; Eich, M.; Moodera, J. S.; Hueso, L. E. *Adv. Mater.* **2014**, *26* (45), 7561−7567.
(8) Datta, S.; Das, B. *Appl. Phys. Lett.* **1990**, *56* (7), 665−667.
(9) Xu, Y.; Awschalom, D. D.; Nitta, J. *Handbook of Spintronics*, 1st ed.; Springer Publishing Company: New York, 2015.
(10) Dietl, T. *Nat. Mater.* **2010**, *9* (12), 965−974.
(11) Picozzi, S. *Front. Phys.* **2014**, *2*, 1−5.

DOI: 10.1021/acs.nanolett.7b04829
Nano Lett. 2018, 18, 2751−2758

(12) Di Sante, D.; Barone, P.; Bertacco, R.; Picozzi, S. *Adv. Mater.* **2013**, *25* (4), 509−513.
(13) Liebmann, M.; Rinaldi, C.; Di Sante, D.; Kellner, J.; Pauly, C.; Wang, R. N.; Boschker, J. E.; Giussani, A.; Bertoli, S.; Cantoni, M.; Baldrati, L.; Asa, M.; Vobornik, I.; Panaccione, G.; Marchenko, D.; Sánchez Barriga, J.; Rader, O.; Calarco, R.; Picozzi, S.; Bertacco, R.; Morgenstern, M. *Adv. Mater.* **2016**, *28* (3), 560−565.
(14) Manchon, A.; Koo, H. C.; Nitta, J.; Frolov, S. M.; Duine, R. A. *Nat. Mater.* **2015**, *14* (9), 871−882.
(15) Hoffmann, A.; Bader, S. D. *Phys. Rev. Appl.* **2015**, *4* (4), 47001.
(16) Rinaldi, C.; Rojas Sánchez, J. C.; Wang, R. N.; Fu, Y.; Oyarzun, S.; Vila, L.; Bertoli, S.; Asa, M.; Baldrati, L.; Cantoni, M.; George, J. M.; Calarco, R.; Fert, A.; Bertacco, R. *APL Mater.* **2016**, *4* (3), 32501.
(17) Nukala, P.; Ren, M.; Agarwal, R.; Berger, J.; Liu, G.; Johnson, A. T. C.; Agarwal, R. *Nat. Commun.* **2017**, *8* (1), 15033.
(18) Krempasky, J.; Weber, A. P.; Pilet, N.; Warnicke, P.; Ebert, H.; Muff, S.; Bisti, F.; Fanciulli, M.; Volfova, H.; Springholz, G.; et al. *Nat. Commun.* **2016**, *7* (May), 13071.
(19) Chattopadhyay, T.; Boucherle, J. X.; VonSchnering, H. G. *J. Phys. C: Solid State Phys.* **1987**, *20* (10), 1431−1440.
(20) Rabe, K. M.; Joannopoulos, J. D. *Phys. Rev. B: Condens. Matter Mater. Phys.* **1987**, *36* (12), 6631−6639.
(21) Deringer, V. L.; Lumeij, M.; Dronskowski, R. *J. Phys. Chem. C* **2012**, *116* (29), 15801−15811.
(22) Wuttig, M.; Lüsebrink, D.; Wamwangi, D.; Wełnic, W.; Gilleßen, M.; Dronskowski, R. *Nat. Mater.* **2007**, *6* (2), 122−128.
(23) Perumal, K. Epitaxial Growth of Ge Sb Te based Phase Change Materials, *Humboldt Universität zu Berlin*, **2013**.
(24) Krempasky, J.; Muff, S.; Pilet, N.; Landolt, G.; Radovi, M.; Shi, M.; Kriegner, D.; Hol, V.; Braun, J.; Dil, J. H.; et al. *Phys. Rev. B: Condens. Matter Mater. Phys.* **2016**, *94*, 205111.
(25) Elmers, H. J.; Wallauer, R.; Liebmann, M.; Kellner, J.; Morgenstern, M.; Wang, R. N.; Boschker, J. E.; Calarco, R.; Sánchez Barriga, J.; Rader, O.; Kutnyakhov, D.; Chernov, S. V.; Medjanik, K.; Tusche, C.; Ellguth, M.; Volfova, H.; Borek, S.; Braun, J.; Minár, J.; Ebert, H.; Schönhense, G. *Phys. Rev. B: Condens. Matter Mater. Phys.* **2016**, *94* (20), 201403.
(26) Oyarzún, S.; Nandy, A. K.; Rortais, F.; Rojas Sánchez, J. C.; Dau, M. T.; Noël, P.; Laczkowski, P.; Pouget, S.; Okuno, H.; Vila, L.; Vergnaud, C.; Beigné, C.; Marty, A.; Attané, J. P.; Gambarelli, S.; George, J. M.; Jaffrès, H.; Blügel, S.; Jamet, M. *Nat. Commun.* **2016**, *7*, 13857.
(27) Gong, S. J.; Yang, Z. Q. *J. Appl. Phys.* **2007**, *102* (3).03370610.1063/1.2767373
(28) Xiao, X. B.; Li, X. M.; Chen, Y. G. *Phys. B* **2009**, *404* (21), 4159−4161.
(29) Zhang, L.; Brusheim, P.; Xu, H. Q. *Phys. Rev. B: Condens. Matter Mater. Phys.* **2005**, *72* (4), 45347.

DOI: 10.1021/acs.nanolett.7b04829
Nano Lett. 2018, 18, 2751−2758